Supporting information

Active site for syngas production by direct partial oxidation of CH$_4$ over ZrO$_2$

Kazumasa Murata*, Keita Arai, Nao Kondo, Ryo Manabe, Takashi Yumura, Saburo Hosokawa*

Mitsubishi Chemical Corporation, 1000 Kamoshida-cho, Aoba-ku, Yokohama 227-8502, Japan

Faculty of Materials Science and Engineering, Kyoto Institute of Technology, Matsugasaki, Sakyo-ku, Kyoto 606-8585, Japan.

Corresponding Author

*E-mail: kazumasa.murata.ma@mcgc.com (Kazumasa Murata), hosokawa@kit.ac.jp (Saburo Hosokawa)

Table S1 POM activities of oxide catalysts at 600°C. Reaction conditions: 100 mg of catalyst, 25% CH_4, 12.5% O_2, N_2 balance (CH_4/O_2 ratio of 2.0), total flow rate of 20 mL/min, total pressure of 1 atm, and contact time of 5.0×10^{-3} g_{cat} min mL^{-1}.

	Conversion (%)		Selectivity (%)					Yield (%)				
	CH_4	O_2	CO	H_2	C_2	CO_2	H_2O	CO	H_2	C_2	CO_2	H_2O
MgO	0.7	0.0	78.0	48.0	0.0	22.0	52.0	0.6	0.3	0.0	0.2	0.3
BaO	0.0	0.0	0.0	15.9	0.0	100.0	84.1	0.0	0.1	0.0	0.0	0.6
Sc_2O_3	30.2	87.6	35.3	33.9	3.8	60.8	62.2	10.3	9.7	1.1	17.8	17.7
Y_2O_3	14.2	41.7	46.3	33.8	3.3	50.4	62.6	6.9	4.8	0.5	7.5	8.8
TiO_2	5.9	13.5	74.2	25.2	0.0	25.8	74.8	3.7	1.0	0.0	1.3	3.0
ZrO_2	29.0	78.2	47.4	41.3	0.3	52.3	58.4	14.0	12.4	0.1	15.5	17.5
YSZ	15.4	38.6	62.8	40.4	0.0	37.1	53.6	10.0	7.5	0.0	6.0	7.5
HfO_2	8.9	26.4	44.0	16.7	0.0	56.0	83.3	3.8	1.3	0.0	4.8	6.2
V_2O_5	1.0	0.0	87.4	0.0	0.0	12.6	100.0	1.0	0.0	0.0	0.1	0.4
Nb_2O_5	0.0	0.0	0.0	0.0	0.0	100.0	100.0	0.0	0.0	0.0	0.1	0.1
Ta_2O_5	27.2	98.5	35.5	3.9	0.0	64.5	96.1	9.4	1.0	0.0	17.1	24.6
MoO_3	0.0	0.0	0.0	0.0	0.0	100.0	100.0	0.0	0.0	0.0	0.0	0.1
WO_3	0.3	0.0	0.0	0.0	0.0	100.0	100.0	0.0	0.0	0.0	0.2	0.1
MnO_2	25.1	100.0	0.0	0.0	0.0	100.0	100.0	0.0	0.0	0.0	24.8	25.8
Fe_2O_3	24.8	100.0	0.0	0.8	0.0	100.0	99.2	0.0	0.2	0.0	24.5	25.7
Co_3O_4	24.1	100.0	0.0	0.0	0.0	100.0	100.0	0.0	0.0	0.0	24.2	25.0
ZnO	10.2	41.4	0.0	7.7	0.7	99.3	91.5	0.0	0.8	0.1	10.5	9.2
Al_2O_3	2.2	6.5	72.5	35.0	0.0	27.5	65.0	2.1	0.7	0.0	0.8	1.4
Ga_2O_3	19.8	74.2	20.3	2.1	2.0	77.7	96.0	3.9	0.4	0.4	15.0	18.9
SiO_2	0.0	0.0	0.0	0.0	0.0	100.0	100.0	0.0	0.0	0.0	0.2	0.3
GeO_2	0.4	0.0	0.0	0.0	0.0	100.0	100.0	0.0	0.0	0.0	0.1	0.1
SnO_2	24.6	100.0	0.0	0.0	0.0	100.0	100.0	0.0	0.0	0.0	23.9	25.1
La_2O_3	8.4	26.1	35.8	40.0	1.8	62.4	58.1	3.3	3.4	0.2	5.8	4.9
CeO_2	25.0	100.0	1.8	5.2	0.0	98.2	94.8	0.4	1.3	0.0	24.4	24.1
Pr_6O_{11}	22.6	90.9	0.0	1.5	2.0	98.0	96.5	0.0	0.4	0.5	22.1	22.2
Nd_2O_3	21.9	70.1	15.3	28.1	5.6	79.0	66.3	3.4	6.3	1.2	17.3	14.8
Sm_2O_3	13.9	41.2	33.7	33.4	3.5	62.8	63.0	4.8	4.6	0.5	8.9	8.6
Eu_2O_3	33.3	98.5	12.4	15.8	19.1	68.5	66.5	4.0	5.6	6.3	22.4	23.5
Gd_2O_3	26.0	74.8	26.1	27.5	11.6	62.3	61.3	6.8	7.5	3.1	16.3	16.7
Dy_2O_3	15.1	43.2	35.9	38.1	3.2	60.9	58.5	5.5	5.6	0.5	9.4	8.7
Yb_2O_3	20.6	56.1	44.2	33.8	6.6	49.2	59.5	9.2	6.9	1.4	10.2	12.2
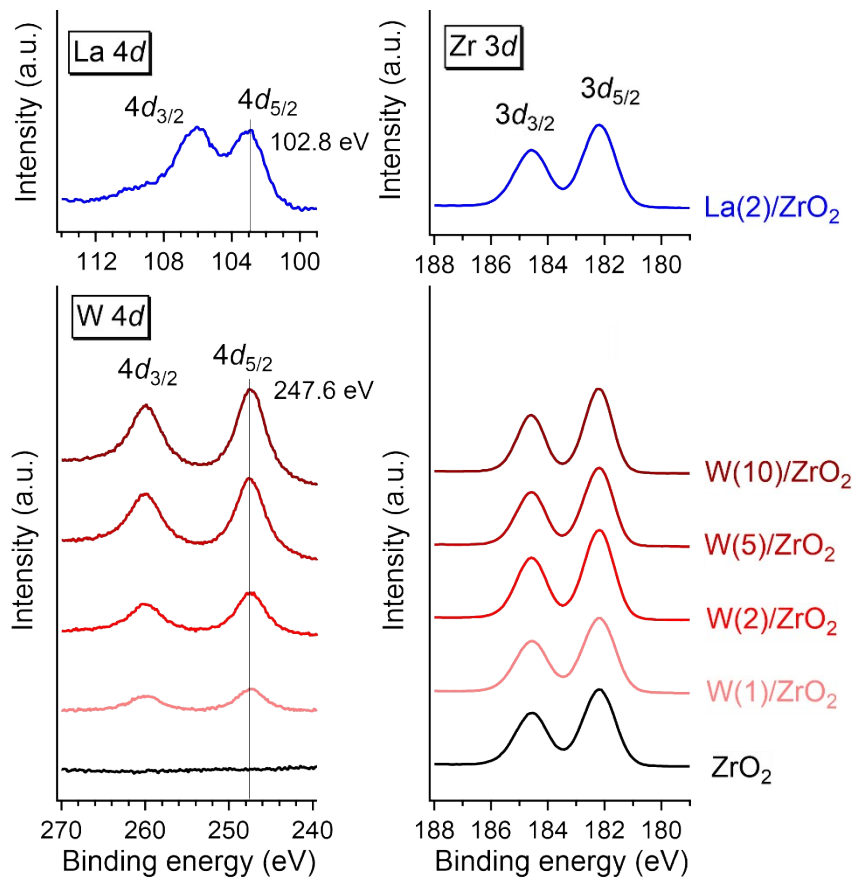
Figure S1 XPS spectra of ZrO$_2$-based catalysts.
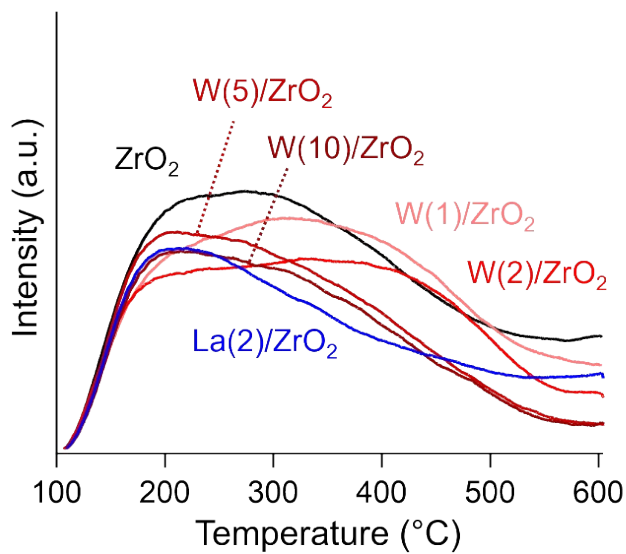
Figure S2 NH$_3$-TPD profiles of ZrO$_2$-based catalysts.
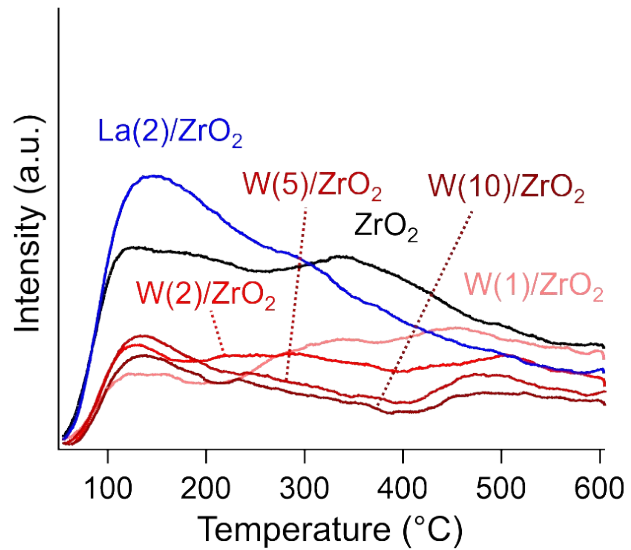
**Figure S3** CO_2-TPD profiles of ZrO_2-based catalysts.
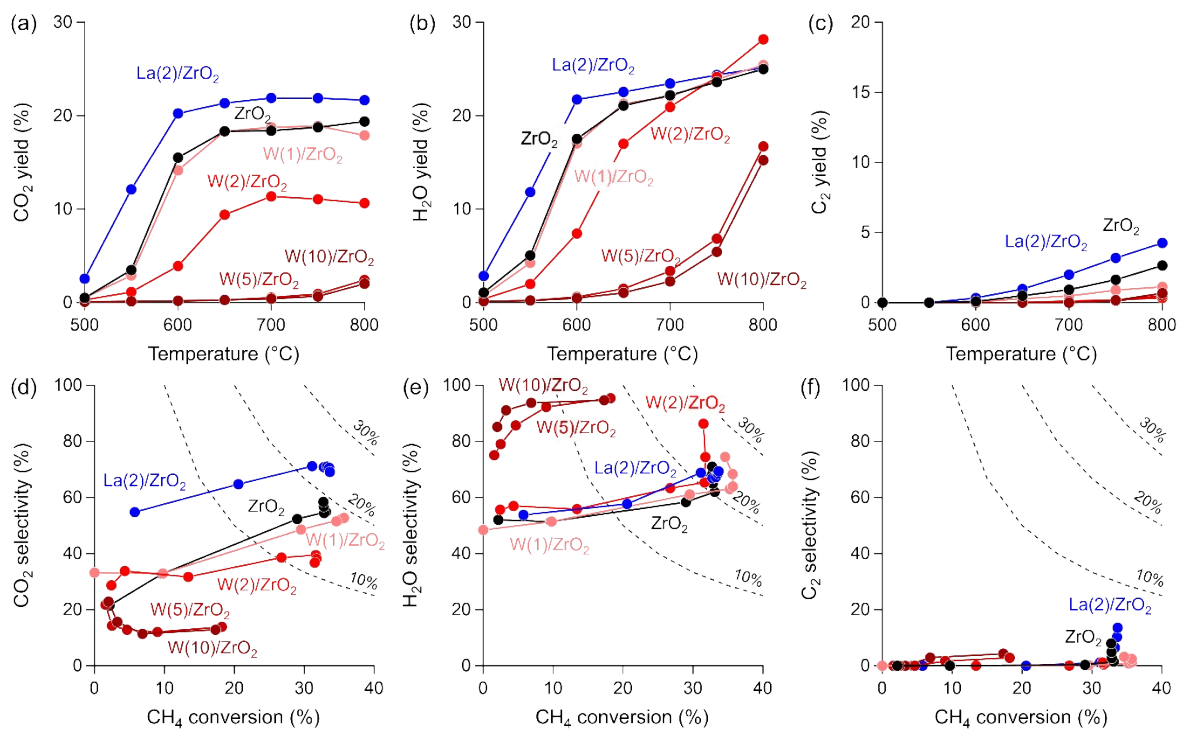
Figure S4 (a) CO_2 yield, (b) H_2O yield, and (c) C2 yield over ZrO_2-based catalysts as functions of temperature. (d) CO_2 selectivity, (e) H_2O selectivity, and (f) C_2 selectivity with CH_4 conversion in POM over ZrO_2-based catalysts. The dotted-line curves show the 10%, 20%, and 30% product yields. Reaction conditions: 100 mg of catalyst, 25% CH_4, 12.5% O_2, N_2 balance (CH_4/O_2 ratio of 2.0), total flow rate of 20 mL/min, total pressure of 1 atm, and contact time of 5.0×10^{-3} g_{cat} min mL^{-1}.
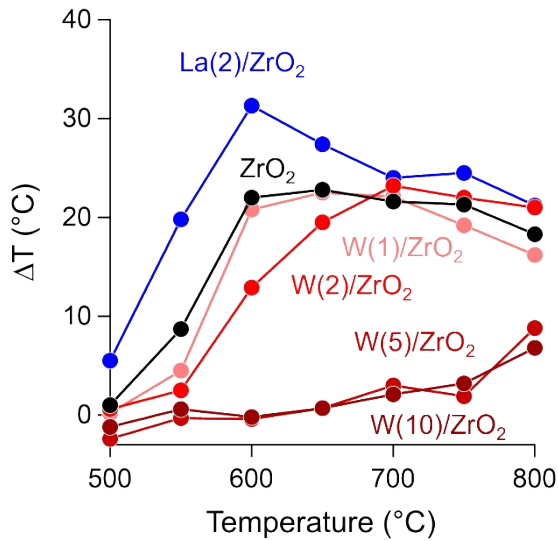
Figure S5 Variation in temperature of catalyst bed against set temperature for POM over ZrO_2-based catalysts. Reaction conditions: 100 mg of catalyst, 25% CH_4, 12.5% O_2, N_2 balance (CH_4/O_2 ratio of 2.0), total flow rate of 20 mL/min, total pressure of 1 atm, and contact time of 5.0×10^{-3} g_{cat} min mL^{-1}.
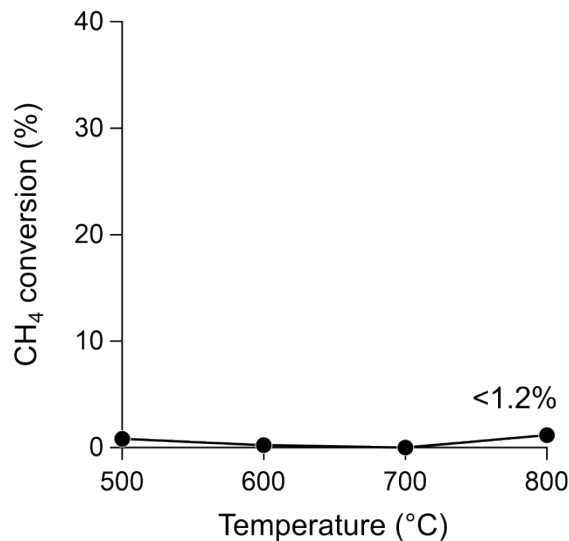
Figure S6 CH_4 conversion in noncatalytic POM as function of temperature. Reaction conditions: 25% CH_4, 12.5% O_2, N_2 balance (CH_4/O_2 ratio of 2.0), total flow rate of 20 mL/min, total pressure of 1 atm, and contact time of 5.0×10^{-3} g_{cat} min mL^{-1}.
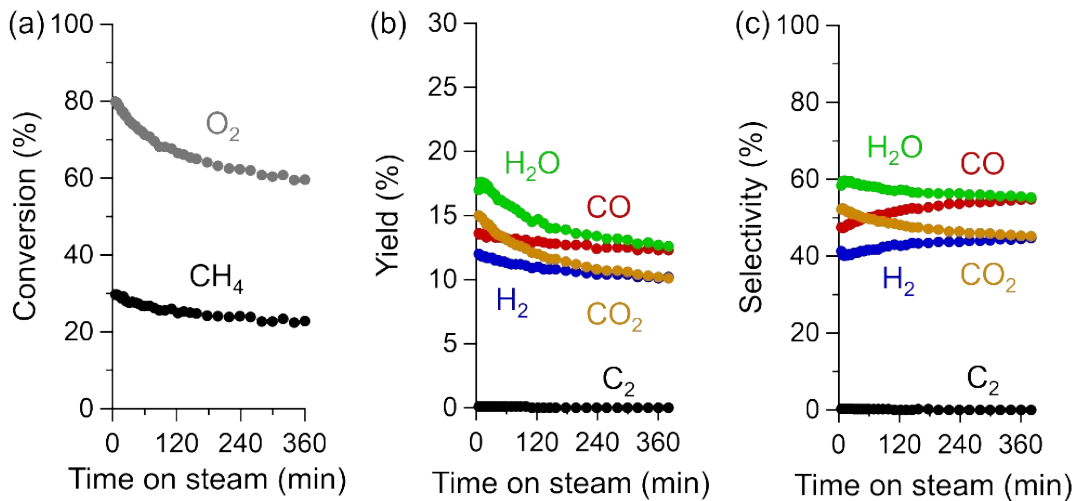
Figure S7 Time on steam of (a) CH_4 and O_2 conversion, (b) product yield, and (c) product selectivity in POM over ZrO_2 catalyst. Reaction conditions: 100 mg of catalyst, 25% CH_4, 12.5% O_2, N_2 balance (CH_4/O_2 ratio of 2.0), total flow rate of 20 mL/min, total pressure of 1 atm, contact time of 5.0×10^{-3} g_{cat} min mL^{-1}, and temperature of 600°C.
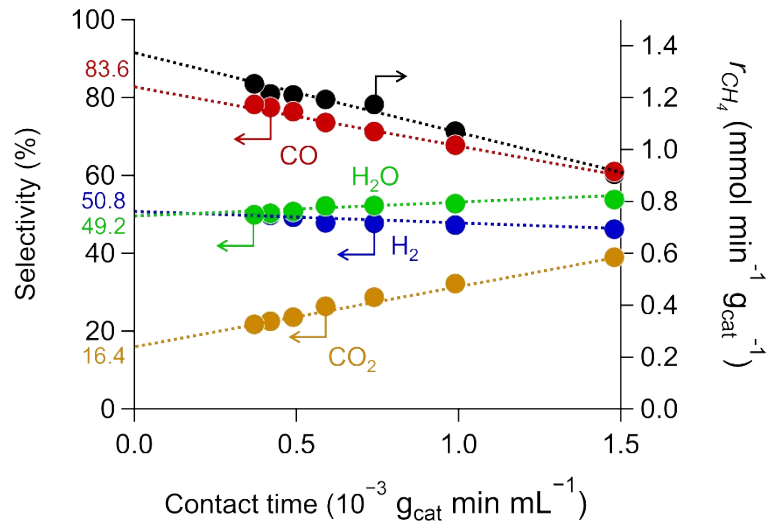

Figure S8 Dependence of product selectivity and CH_4 oxidation rate on contact time in POM over ZrO_2 catalyst. Reaction conditions: 10 mg of ZrO_2 catalyst, 30% CH_4, 15% O_2, N_2 balance (CH_4/O_2 ratio of 2.0), total flow rate of ~27 mL/min, total pressure of 1 atm, and temperature of 600°C.

6
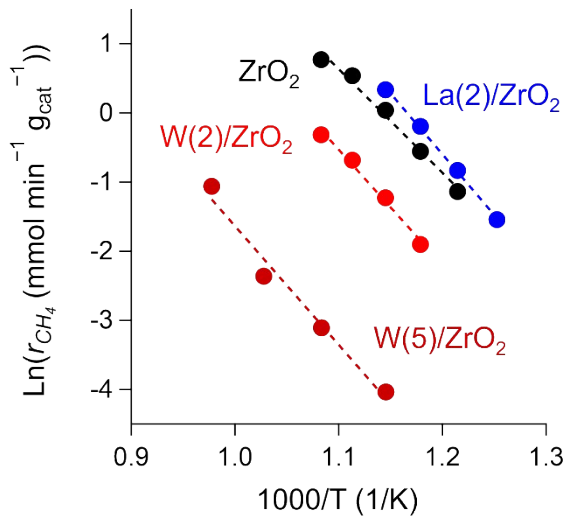
Figure S9 Arrhenius plots of CH_4 oxidation rate of ZrO_2-based catalysts for POM. Reaction conditions: 25% CH_4, 12.5% O_2, N_2 balance (CH_4/O_2 ratio of 2.0), total flow rate of 20 mL/min, and total pressure of 1 atm.

Table S2 Vibrational frequencies of reaction intermediates species on ZrO_2-based catalysts.

| Wavenumber (cm^{-1})	Species	Vibrational mode	Reference
3800–2500	H_2O (adsorbed water)	ν(OH)	[1,2]
3780–3760	Terminal OH (t-OH)	ν(OH)	[3–8]
3740–3730	Bridged OH (b-OH)	ν(OH)	[6,7]
3680–3660	Multicoordinated OH (m-OH)	ν(OH)	[3–8]
3630–3620	Monodentate bicarbonate (HCO_3–)	ν(OH)	[3,6,8,9]
3014	CH_4 (gas)	ν_a(CH)	[10]
2965–2955	Bidentate formate (b-HCOO–)	ν_a(OCO) + ν_s(OCO) and δ(CH) + ν_s(OCO)	[3–5,7–12]
2885–2870	Bidentate formate (b-HCOO–)	ν(CH)	[3–5,7–12]
1640–1600	Monodentate bicarbonate (m-HCO_3–)	ν_a(OCO)	[3,6,8,9]
	Bridged carbonate (br-CO_3–)	ν_a(OCO)	[9]
1590–1550	Bidentate formate (b-HCOO–)	ν_a(OCO)	[3–5,9–12]
	Bidentate carbonate (b-CO_3–)	ν_a(OCO)	[3,8]
1470–1430	Monodentate bicarbonate (m-HCO_3–)	ν_s(OCO)	[3,6,9]
	Terminal CH_3O– (t-CH_3O–)	δ(CH)	[4,5,10,13,14]
	Polydentate carbonate (p-CO_3–)	ν_a(OCO)	[9,12]
1400–1320	Bidentate formate (b-HCOO–)	δ(CH) and ν_s(OCO)	[3–5,7–12]
	Polydentate carbonate (p-CO_3–)	ν_s(OCO)	[9,12]
	Bidentate carbonate (b-CO_3–)	ν_s(OCO)	[3,8]
	Bridged carbonate (br-CO_3–)	ν_s(OCO)	[9]
1304	CH_4 (gas)	δ(CH)	[10]
1150–1130	Terminal CH_3O– (t-CH_3O–)	ν(CO)	[4,5,10,13,14]
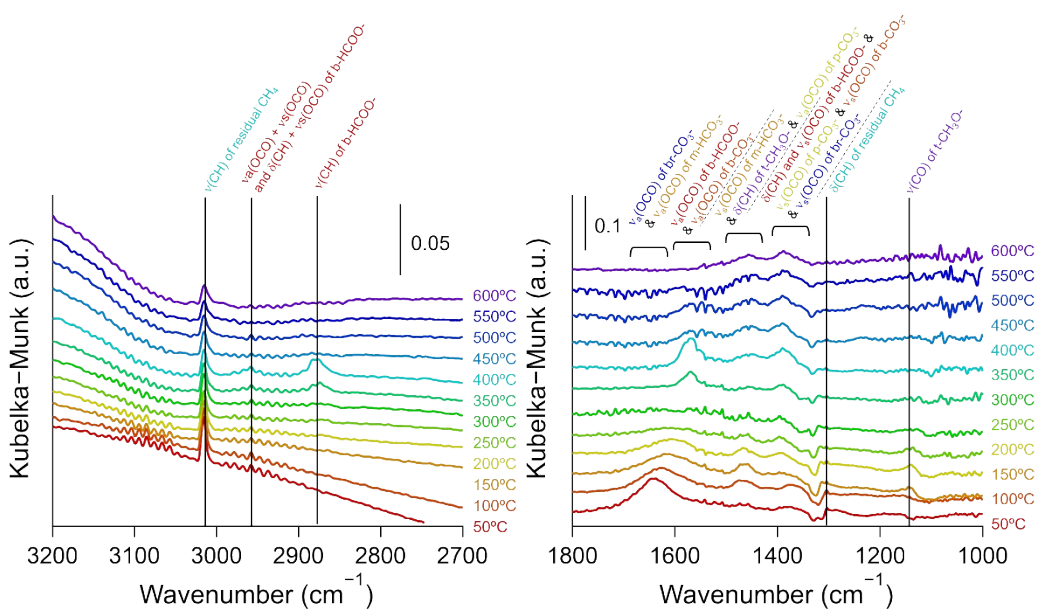
Figure S10 In situ DRIFTS spectra of ZrO_2 catalyst in Ar flow after POM.
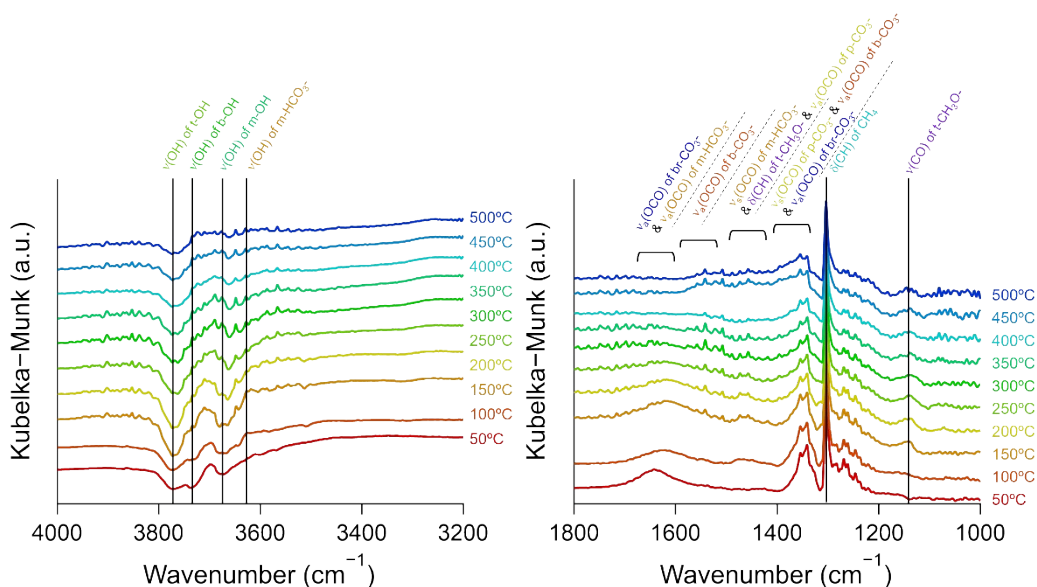

Figure S11 In situ DRIFTS spectra of ZrO_2 catalyst in 25% CH_4/N_2 flow.
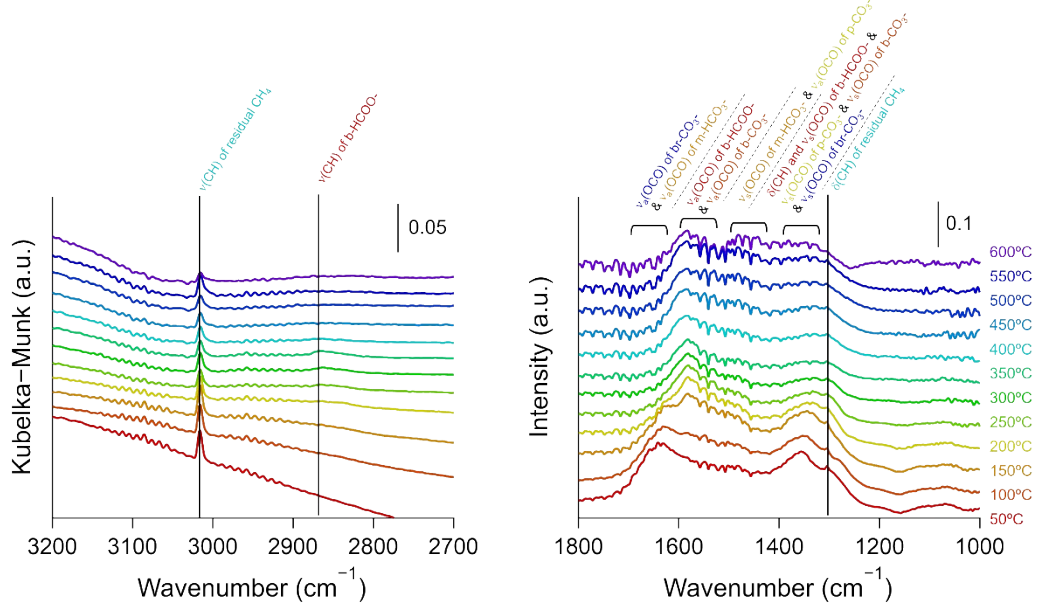
Figure S12 In situ DRIFTS spectra of La(2)/ZrO$_2$ catalyst in Ar flow after POM.
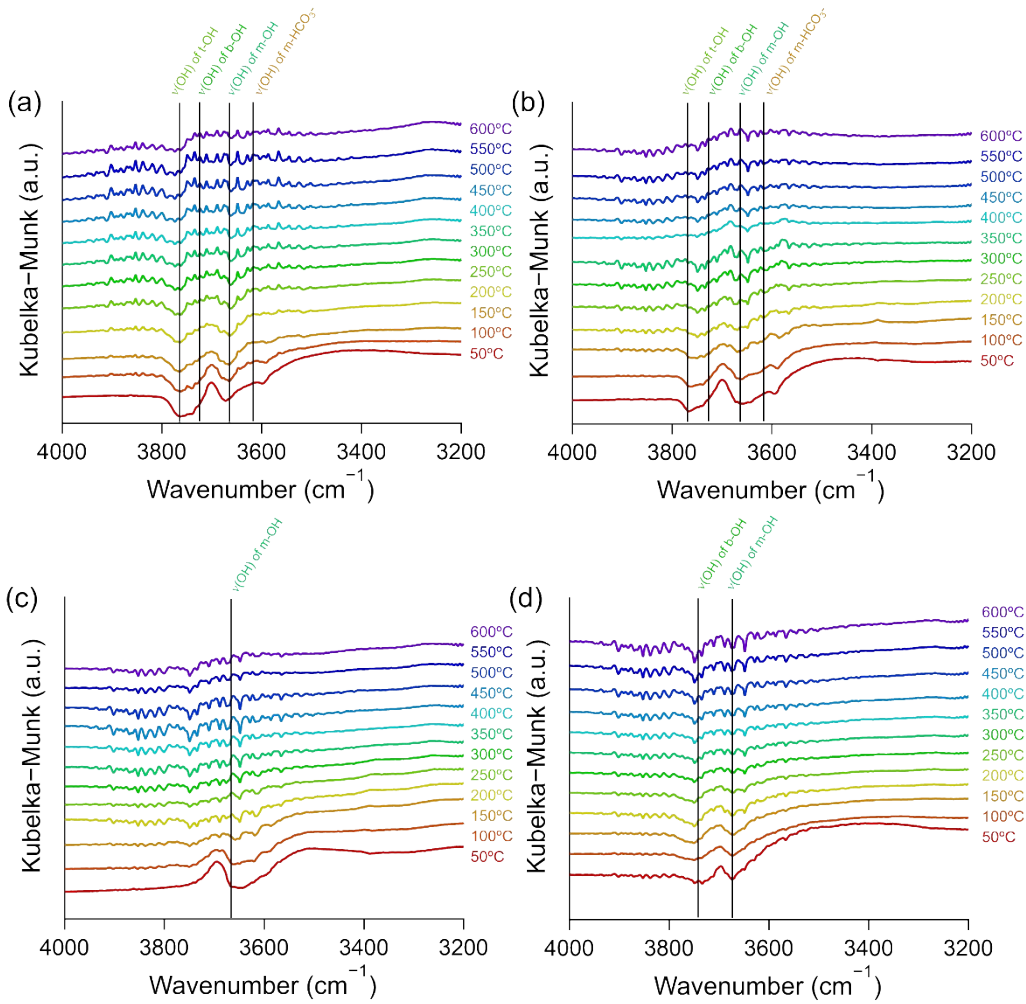
Figure S13 In situ DRIFTS spectra of ZrO$_2$-based catalysts during POM: (a) W(1)/ZrO$_2$, (b) W(2)/ZrO$_2$, (c) W(5)/ZrO$_2$, and (d) La(2)/ZrO$_2$. Reaction conditions: 25% CH$_4$, 12.5% O$_2$, N$_2$ balance (CH$_4$/O$_2$ ratio of 2.0), total flow rate of 40 mL/min, and total pressure of 1 atm.

DFT setting and modeling of ZrO$_2$ catalyst

To model the ZrO$_2$ catalyst, we considered its monoclinic phase and ($\bar{1}$11) surfaces which were energetically stable. A 2 × 2 × 1 monoclinic ($\bar{1}$11) ZrO$_2$ surface containing Zr$_{48}$O$_{96}$ was constructed, as shown in Figure S14. A vacuum spacing of 16 Å was added along the *c* axis, which was large enough to prevent interactions between each surface model along the axis. Using the monoclinic ZrO$_2$ model, we optimized the atomic configurations of the local minima and transition states during methane activation. In supercell calculations, Brillouin zone sampling was restricted to the Γ point, and energies were converged at a 1.0×10^{-5} eV tolerance. To identify the transition states, we adopted the CI–NEB method using four intermediate images. The local minima and transition states in methane activation were optimized by fixing the lattice parameters in the surface supercell, fully relaxing the positions of the atoms contained in an upper layer, and fixing those of the atoms in the bottom layer (inside the red rectangle in Figure S14). The optimization was deemed to have converged when the maximum forces on all atoms were less than 0.05 eV/Å.
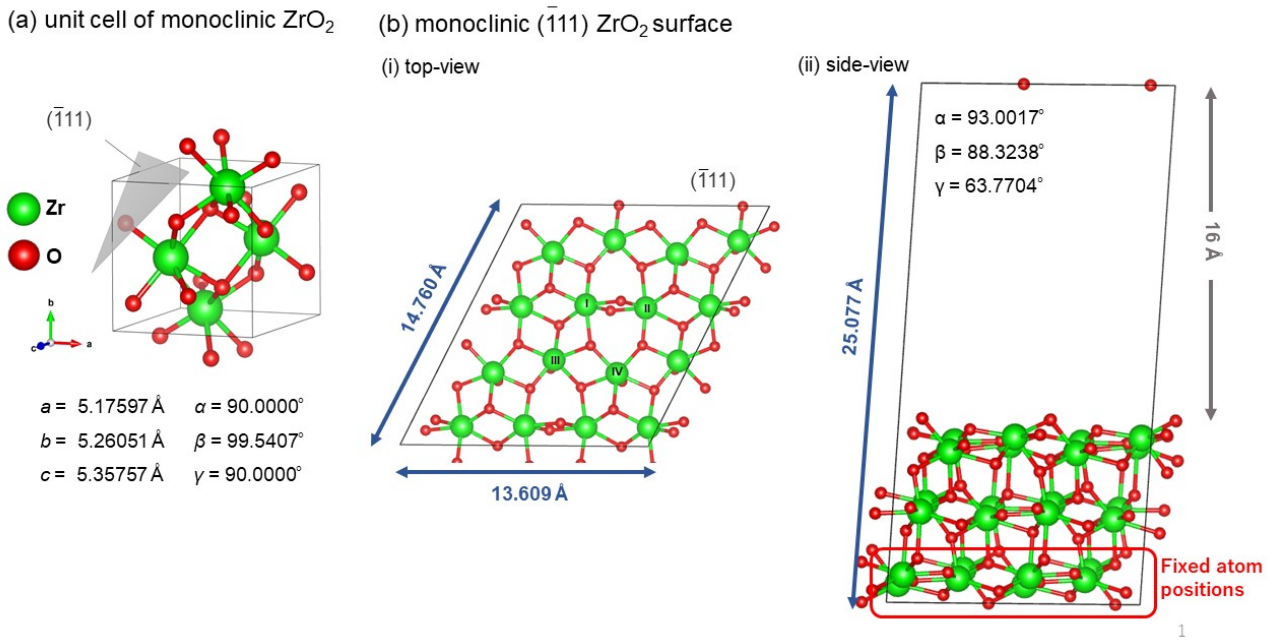

Figure S14 (a) Unit cell of studied monoclinic ZrO$_2$ and (b) its surface. The Zr atoms labeled I, III, and IV were coordinated by six oxygen atoms, and the Zr atom labeled II was coordinated by seven oxygen atoms. Accordingly, coordinatively unsaturated Zr atoms, labeled I, III, and IV, enabled the binding of H$_2$O molecules in the atmosphere to the Zr atoms, thus generating HO-attached ZrO$_2$ surfaces with oxygen monovacancies.

12

Table S3 Geometric changes in methane before and after its interaction with oxygen-deficient ZrO_2 surface, obtained via PBE DFT calculations.

	Methane	Methane bound to oxygen-deficient ZrO_2 surface
B[C–H(a)] [a]	1.096	1.100
B[C–H(b)] [a]	1.096	1.099
B[C–H(c)] [a]	1.096	1.096
B[C–H(d)] [a]	1.096	1.094
A[H(b)–C–H(a)] [b]	109.5	112.5
A[H(b)–C–H(d)] [b]	109.5	109.2
A[H(b)–C–H(c)] [b]	109.5	108.4
A[H(a)–C–H(d)] [b]	109.5	108.7
A[H(a)–C–H(c)] [b]	109.5	107.6
A[H(d)–C–H(c)] [b]	109.5	110.4

[a] B indicates the bond lengths (Å) between the atoms in the parentheses.

[b] A indicates the angles (°) between the atoms in the parentheses.

References

(1)   Sagadevan, S.; Podder, J.; Das, I. *J. Mater. Sci. Mater. Electron.* **2016**, *27*, 5622–5627.

(2)   Ishikawa, H.; Kondo, J. N.; Domen, K. *J. Phys. Chem. B* **1999**, *103*, 3229–3234.

(3)   Kondo, J.; Abe, H.; Sakata, Y.; Maruya, K. I.; Domen, K.; Onishi, T. *J. Chem. Soc. Faraday Trans.* **1988**, *84*, 511–519.

(4)   Ouyang, F.; Kondo, J. N.; Maruya, K.; Domen, K. *J. Phys. Chem. B* **1997**, *101*, 1–3.

(5)   Ouyang, F.; Nakayama, A.; Tabada, K.; Suzuki, E. *J. Phys. Chem. B* **2000**, *104*, 2012–2018.

(6)   Bachiller-Baeza, B.; Rodriguez-Ramos, I.; Guerrero-Ruiz, A. *Langmuir* **1998**, *14*, 3556–3564.

(7)   Kouva, S.; Honkala, K.; Lefferts, L.; Kanervo, J. *Catal. Sci. Technol.* **2015**, *5*, 3473–3490.

(8)   Kouva, S.; Andersin, J.; Honkala, K.; Lehtonen, J.; Lefferts, L.; Kanervo, J. *Phys. Chem. Chem. Phys.* **2014**, *16*, 20650–20664.

(9)   Ko, E.; Kogler, M.; Bielz, T.; Klo, B.; Penner, S. *J. Phys. Chem. C* **2013**, *117*, 17666–17673.

(10)   He, Y.; Guo, F.; Yang, K. R.; Heinlein, J. A.; Bamonte, S. M.; Fee, J. J.; Hu, S.; Suib, S. L.; Haller, G. L.; Batista, V. S.; Pfefferle, L. D. *J. Am. Chem. Soc.* **2020**, *142*, 17119–17130.

(11)   Zhu, J.; Van Ommen, J. G.; Lefferts, L. *J. Catal.* **2004**, *225*, 388–397.

(12)   Jung, K.; Bell, A. T. *J. Catal.* **2000**, *193*, 207–223.

(13)   Wu, C.; Lin, L.; Liu, J.; Zhang, J.; Zhang, F.; Zhou, T.; Rui, N.; Yao, S.; Deng, Y.; Yang, F.; Xu, W.; Luo, J.; Zhao, Y.; Yan, B.; Wen, X. D.; Rodriguez, J. A.; Ma, D. *Nat. Commun.* **2020**, *11*, 5767.

(14)   Binet, C.; Daturi, M. *Catal. Today* **2001**, *70*, 155–167.

(15)   Ko, E.; Kogler, M.; Bielz, T.; Klötzer, B.; Penner, S. *J. Phys. Chem. C* **2013**, *117*, 17666–17673.